Systems/Circuits

Timing-Dependent Potentiation and Depression of Electrical Synapses Contribute to Network Stability in the Crustacean Cardiac Ganglion

Daniel R. Kick and David J. Schulz
Division of Biological Sciences, University of Missouri–Columbia, Columbia, Missouri 65211

Central pattern generators produce many rhythms necessary for survival (e.g., chewing, breathing, locomotion), and doing so often requires coordination of neurons through electrical synapses. Because even neurons of the same type within a network are often differentially tuned, uniformly applied neuromodulators or toxins can result in uncoordinated activity. In the crab (*Cancer borealis*) cardiac ganglion, potassium channel blockers and serotonin cause increased depolarization of the five electrically coupled motor neurons as well as loss of the normally completely synchronous activity. Given time, compensation occurs that restores excitability and synchrony. One of the underlying mechanisms of this compensation is an increase in coupling among neurons. However, the salient physiological signal that initiates increased coupling has not been determined. Using male *C. borealis*, we show that it is the loss of synchronous voltage signals between coupled neurons that is at least partly responsible for plasticity in coupling. Shorter offsets in naturalistic activity across a gap junction enhance coupling, whereas longer delays depress coupling. We also provide evidence on why a desynchronization-specific potentiation or depression of the synapse could ultimately be adaptive through using a hybrid network created by artificially coupling two cardiac ganglia. Specifically, a stray neuron may be brought back in line by increasing coupling if its activity is closer to the remainder of the network. However, if a the activity of a neuron is far outside network parameters, it is detrimental to increase coupling, and therefore depression of the synapse removes a potentially harmful influence on the network.

Key words: central pattern generator; electrical synapse; gap junction; homeostatic plasticity; plasticity

Significance Statement

Understanding how neural networks maintain output over years despite environmental and physiological challenges requires understanding the regulatory principles of these networks. Here, we study how cells that are synchronously active at baseline respond to becoming desynchronized. In this system, a loss of synchrony causes different parts of the heart to receive uncoordinated stimulation. We find a calcium-dependent control mechanism that alters the strength of electrical connections between motor neurons. Although others have described similar control mechanisms, here, we demonstrate that voltage changes are sufficient to elicit regulation. Furthermore, we demonstrate that strong connections in a sufficiently perturbed network can prevent any neuron from producing its target activity, thus suggesting why the connections are not constitutively as strong as possible.

Introduction

Electrical synapses are dynamic structures capable of activity-dependent plasticity (Haas et al., 2016) and reshaping circuit behavior (Marder et al., 2017; Alcamí and Pereda, 2019). Electrical synapses are integral to functions including escape behavior (Allen et al., 2006), visual encoding (Wang et al., 2017), and retinal processing (Kothmann et al., 2012). Electrical synapses undergo long-term potentiation (eLTP) or long-term depression (eLTD) because of changes in phosphorylation of the gap junction (Wang et al., 2015; Sevetson et al., 2017). Often metabotropic glutamatergic signaling through group 2 mGluR activation results in eLTP, whereas group 1 activation results in eLTD (Wang et al., 2015).

The past decade has yielded evidence suggestive of a voltage-dependent modulation of electrical synapses. The thalamic reticular nucleus (TRN) undergoes eLTD or eLTP following evoked bursting (Haas et al., 2011) or spiking (Fricker et al., 2020).

Received Sep. 14, 2020; revised July 14, 2022; accepted July 19, 2022.

Author contributions: D.R.K. and D.J.S. designed research; D.R.K. and D.J.S. performed research; D.R.K. and D.J.S. contributed unpublished reagents/analytic tools; D.R.K. and D.J.S. analyzed data; D.R.K. and D.J.S. wrote the paper.

This work was supported by National Institutes of Health Grant R01MH046742-29 and National Institute of General Medical Sciences Grant T32GM008396-26 (D.R.K.).

The authors declare no competing financial interests.

Correspondence should be addressed to David J. Schulz at schulzd@missouri.edu.

https://doi.org/10.1523/JNEUROSCI.2402-20.2022

Copyright © 2022 the authors

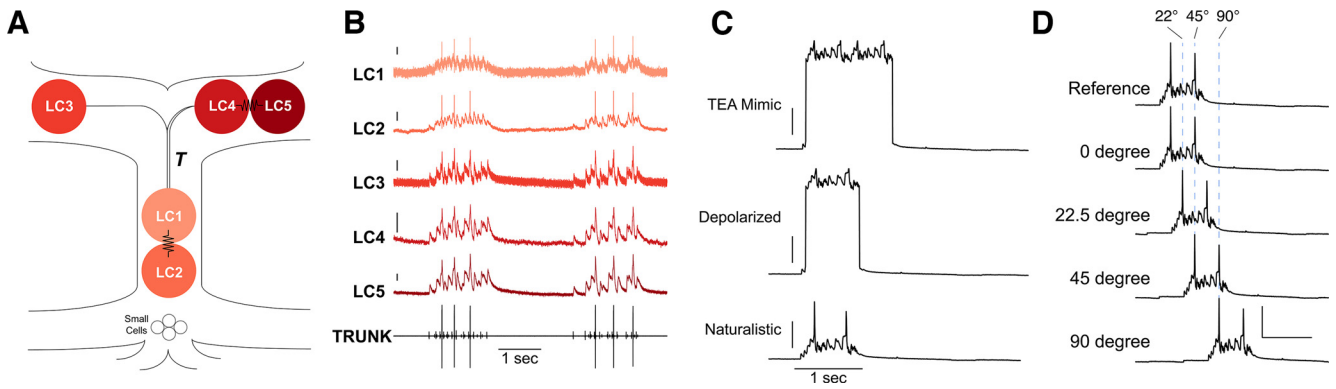

Figure 1. Synchronous, normative LC depolarizations can be manipulated through network silencing followed by voltage clamp. ***A***, The five motor neurons (LCs) of the cardiac ganglion are driven by four pacemaker interneurons (Small Cells) through chemical and electrical synaptic excitation. ***B***, LCs depolarize synchronously, as shown by simultaneous intracellular recordings. A simultaneous extracellular recording made from the nerve Trunk (T in ***A***) detects three LC action potentials per burst (large events) as well as the pacemaker activity of the Small Cells (small events). Calibration: 2 mV. ***C***, After Small Cells are silenced by displacing physiological saline with isotonic sucrose, fictive LC activity patterns can be induced with a two-electrode voltage clamp. Fictive activity patterns are designed to mimic (1) the effects of TEA (TEA Mimic), (2) aberrantly high depolarization without increased length of the depolarization (Depolarized), and (3) normative activity using a single standardized waveform (Naturalistic). Calibration: 10 mV. ***D***, Experimentally controlled shifts from synchronous activity using the Naturalistic protocol across two LCs are expressed as phase angles where an offset of one-fourth the period is 90°. Protocols with delays between LCs ranging from 0 to one-fourth of the period were created with the Naturalistic stimulus.

Evoked spiking has been shown to cause eLTP in *Hirudo medicinalis* (Welzel and Schuster, 2018). The TRN results suggest a depolarization-dependent sign change, and it has been proposed that this is regulated via intracellular calcium (Sevetson et al., 2017; Fricker et al., 2020). However, these experiments have not been conducted with mGluR antagonists, and the complexity of the circuits involved make it challenging to disentangle potential voltage-dependent effects from metabotropic ones. Regardless, these studies provide compelling support for the possibility of a voltage-dependent mechanism of eLTP and eLTD. In this study, for the first time we address two provocative ideas put forward in this field in recent years: whether "the activity of electrical synapses themselves lead to their potentiation" (Haas et al., 2016) and whether "activity-dependent LTD could be a mechanism used by a single bursting cell to unplug from ... [a] network" (Haas and Landisman, 2012).

We address these questions using the *Cancer borealis* cardiac ganglion (CG), which contains five motor neurons [large cells (LCs); Cooke, 2002] that depolarize synchronously (Fig. 1*A*,*B*). Waveform synchrony occurs despite twofold to fourfold variability in conductance magnitudes within LCs of a network (Ransdell et al., 2013) through a tuning of membrane conductances (Lane et al., 2016), electrical coupling (Watanabe, 1958), and synchronous excitation. Pharmacological blockade of potassium channels with tetraethylammonium (TEA) results in hyperexcitability, increased activity (Ransdell et al., 2012), and desynchronized waveforms of these coupled cells (Ransdell et al., 2013). However, within 30–60 min of this loss of synchrony, increased coupling (eLTP), in conjunction with an increase in A-type potassium conductance, acts to restore synchrony in a compensatory fashion (Lane et al., 2016). However, it is not clear whether asynchronous voltage across the electrical synapses, increased depolarization, or both are the salient signals initiating the response that enhances coupling.

We hypothesized that voltage across the gap junction, coincident with depolarization, is a relevant electrophysiological signal for coupling modulation. Investigating these mechanisms requires decoupling the increased depolarization/excitability TEA causes from signal synchrony. We accomplish this experimentally using a two-electrode voltage clamp to precisely and independently control the membrane voltage of coupled cells. After suspending network activity, cells are clamped to the same activity with or without a delay between them.

We first replicated the findings of the TEA block results (Lane et al., 2016) without pharmacology using protocols that mimic depolarization levels seen in TEA. We show that eLTP only occurs when asynchronous activity is present and that this phenomenon is calcium dependent. Next, we demonstrated that increased depolarization is not necessary to alter coupling; at typical burst amplitudes, asynchronous activity elicits plasticity. Further, the sign of the change (i.e., potentiation or depression) is dependent on the delay between cells, with a short delay resulting in eLTP and a long delay resulting in eLTD. Finally, we use hybrid networks of two independent CGs with a simulated electrical synapse connecting one LC in each network to show a potential benefit for the induction of eLTP at lesser degrees of loss of synchrony and eLTD when loss of synchrony is more severe.

Materials and Methods

Animals

Wild-caught adult male Jonah crabs (*Cancer borealis*) were purchased from the Fresh Lobster Company. On arrival, animals were housed in tanks maintained at 12°C until use. Crabs were anesthetized before use by cold exposure for 30 min. The heart was removed from the animal and microdissected to isolate the ganglion, which was pinned out in a Sylgard lined dish. Motor neurons were exposed by removing the connective sheath around them with a fine pin. During the dissection, the preparation was bathed in chilled physiological saline containing the following (in mM): 440 NaCl, 26 MgCl2, 13 CaCl2, 11 KCl, and 10 HEPES, pH 7.4–7.5. All chemicals were purchased from Fisher Scientific unless stated otherwise.

Electrophysiology

Recordings and measurements. The cardiac ganglion in *C. borealis* consists of nine neurons (Fig. 1*A*). Four interneurons, small cells (SCs), form a pacemaking kernel that excites the five LC motor neurons in precise synchrony to generate action potentials that drive muscle contraction (Fig. 1*A*,*B*). Paired LC somata are found in an anterior branch of the network (Fig. 1*A*), and among these paired somata are strong local electrical synapses that are the focus of these studies (Lane et al., 2016, 2018). A petroleum jelly well around the posterior bifurcation isolated

the small cells (Fig. 1*A*), and a section of ganglionic trunk from the anterior LCs (i.e., LC3–5; Fig. 1*A*,*B*). This was used for recording network activity extracellularly with stainless steel electrodes connected to a differential AC amplifier (model 1700, A-M Systems). Desheathed somata of LC4 and LC5 were recorded from using sharp electrodes filled with 3 M KCl (4–16 MΩ). Following baseline recordings, physiological saline around the small cells was displaced by isotonic sucrose (750 mM) to suspend network activity as described previously (Lane et al., 2016). When isotonic sucrose failed to fully suppress activity, tetrodotoxin (10^{-4} mM) was added dropwise until residual activity was eliminated. When measurements of baseline activity were not required, networks were sometimes silenced by cutting the trunk of the network to immediately and irreversibly remove SC input from the LCs.

Gap junction and membrane resistances. Two-electrode current- and voltage-clamp protocols were used to measure input resistance (R_{in1} or R_{11}) and coupling resistance (g_j^{-1}), or the resistance across the electrical synapse. To measure these with current clamp, we used sequential current injections (of sufficient length for the voltage to reach steady state) into both LCs. This protocol consisted of five sweeps, where one cell received 0 nA (250 ms), −6 nA (1500 ms), and 0 nA (2999 ms) and the other 0 nA (2999 ms), −6 nA (1500 ms), and 0 nA (250 ms). Initially −2 nA pulses were used, but −6 nA proved to offer a better signal-to-noise ratio. From the resulting traces we calculated input resistance ($R_{in1} = R_{11} = \frac{\Delta V_1}{I_1}$), membrane resistance ($R_1 = \frac{R_{in1} \cdot R_{in2} - R_{12}^2}{R_{in2} - R_{12}}$), and coupling coefficient ($CC_{12} = \frac{\Delta V_2}{\Delta V_1}$). We restrict our consideration of these parameters to membrane resistance (R_1) and coupling coefficient (CC_{12} or CC). Here, subscripts 1 and 2 denote the presynaptic and postsynaptic cells, respectively. Each of these was measured bidirectionally for a given pair of cells. These formulas are reported in (Bennett, 1966).

We measure coupling resistance more directly via voltage clamp. One cell was held at −60 mV, whereas the other was stepped to a test voltage. Specifically, we clamped both cells to −60 mV (250 ms) then clamped one at a test voltage ranging from −80 mV to −40 mV in increments of 5 mV (1000 ms). After the test step, we clamped both cells to −60 mV and then stepped the other cell to the same voltage steps. The −60 mV step was excluded from consideration as it resulted in no transjunctional voltage. From this, coupling conductance can be derived as follows: ($g_j = \frac{I_2}{V_2 - V_1}$) (Spray et al., 1979). The reciprocal of g_j, g_j^{-1}, is coupling resistance. We found a close correspondence between R_c and g_j^{-1} (data not shown), and for simplicity, we focus on gj^{-1}.

The above protocols were created and run in Clampex 10.7 software (Molecular Devices) using two AxoClamp-2A intracellular amplifiers (Molecular Devices), a Brownlee precision amplifier (model 410) for preamplification of the current injecting channels, and a Digidata 1440A digitizer (Molecular Devices).

Stimulus protocols delivered via voltage clamp. Following baseline measurements, LCs were voltage clamped to a waveform with increased depolarization or a naturalistic waveform. To mimic the effects of TEA on LC waveforms (Ransdell et al., 2013; Lane et al., 2016), we created a TEA Mimic stimulus protocol (Fig. 1*C*, TEA Mimic) consisting of a high-voltage, long-duration pulse (depolarization to approximately −18 mV, an increase of 35 mV from a resting membrane potential of −53 mV for 1.61 s) followed by a return to baseline. This stimulus protocol was applied continuously except hen measurements were being taken. This protocol was derived from a control LC waveform, where the depolarization was doubled in length and increased by 30 mV. Spike transients were removed to prevent excessive depolarization, which left a shape more akin to an extreme TEA waveform. To mimic the TEA-induced desynchronization reported previously (Ransdell et al., 2013), we introduced a delay of 0.59 s between the two voltage protocols (Fig. 2*A*, ASYNC).

The desynchronized TEA Mimic protocol still contains overlap in the on phases between cells, resulting in a portion of the stimulus where there is no transjunctional voltage difference. Some TEA responses documented show little overlap in the depolarization phases of anterior LCs (i.e., LC3 vs LC4/5; (Ransdell et al., 2013, their Figs. 1E, 2A2,2A3). Therefore, we designed a second protocol that resembles the TEA waveform but with a shorter depolarization time, which eliminated overlap in the timing of the on phase between cells. In this Depolarized protocol (Fig. 1*C*), the on phase amplitude was consistent with the previous protocols (~34 mV from baseline) but remained elevated only for ~0.80 s, half as long as the depolarization in the TEA Mimic protocol. Once again, we did not allow voltages above −14 mV to prevent excessive depolarization of spike transients. The delay between onset of depolarization between cells was 0.98 s, one-fourth the period, or 90°. With this delay, there is no overlap between the on phases of the two stimuli in the two separate cells.

We then performed experiments with a treatment that more closely resembles natural, endogenous activity. To do so, we silenced preparations with isotonic sucrose, and then we used a standardized trace of natural control activity to serve as the voltage command for voltage-clamp protocols across preparations (Fig. 1*C*, Naturalistic protocol). For asynchronous stimuli, a phase angle was introduced by shifting the voltage with respect to the time. Here, phase is defined as a fraction of the period (e.g., a phase angle of 90° for a cell with a 4 s period is equivalent to a 1 s delay). Representative phase angles used are shown in Figure 1*D*. These protocol manipulations were accomplished through a combination of operations in R (https://www.R-project.org/) and Microsoft Excel with the resultant time-voltage pairs exported as text files. Stimulus protocols were used to drive LC4 and LC5 for 1 h, with the above measurements collected every 20 min and with each preparation exposed to a single stimulus protocol type.

Dynamic clamp protocols. To assess the functional consequences of desynchronization between cells in an ongoing rhythm, we created a dynamic clamp protocol in NetClamp (Gotham Scientific) that simulated a bidirectional electrical synapse between LC3s in two cardiac ganglia. We then set the strength of this synapse to 0, 0.025, 0.05, 0.1, 0.15, or 0.2 ms, consistent with conductances previously tested in this system (Lane et al., 2016). The simulated electrical synapse connected LC3 in the cardiac ganglia of two animals (see Fig. 4). Gap-free recordings of the voltage in both cells, and extracellular recordings capturing small cell pacemaker activity, were collected from both networks and processed as described below. Note that although we compute the delay between burst onset, conversion to phase angle is not appropriate because of cycle-to-cycle variability in period.

Experimental design and statistical analysis

Experimental design. We designed the initial set of these experiments as a simple comparison of two groups, TEA Mimic synchronously applied versus applied with a delay. We repeated this experiment with a shorter duty cycle and used it to assess whether influx of calcium is necessary by using a high-amplitude protocol in the absence and presence of cadmium chloride (250 μM Cd^{2+}).

In the next set of experiments, we removed the depolarizing aspect of the treatment while varying desynchronization. We varied the delay between a single protocol, based on a recording collected in control saline, using four phase angles of 0, 22.5, 45, 90° (i.e., a delay of the 0, 1/16th, 1/8th, or 1/4th times the period).

Finally, we used dynamic clamp to vary the strength of fictive coupling between two cells of different networks at six levels (0, 0.025, 0.05, 0.1, 0.15, and 0.2 μs). We allowed delay between networks to vary as a second factor. Because of period variability within a network and between the two networks, this factor is treated as being continuous. We sought two sets of networks so that one set possessed similar activity, whereas the other set had mismatched activity. This final experiment is designed to be qualitatively rather than quantitatively assessed.

None of the experiments presented here were preregistered. No statistical procedure was used to determine sample size. We based the sample size on those efficacious for detecting similar effects in prior publications (Ransdell et al., 2012, 2013; Lane et al., 2016).

Data preprocessing. Measurements of voltage and current change or steps were obtained with Clampfit version 10.7 and aggregated in Microsoft Excel before being loaded into R (https://cran.r-project.org/web/packages/readxl/index.html) for analysis. Coupling conductance (g_j) was represented as coupling resistance (g_j^{-1}). Data were quality

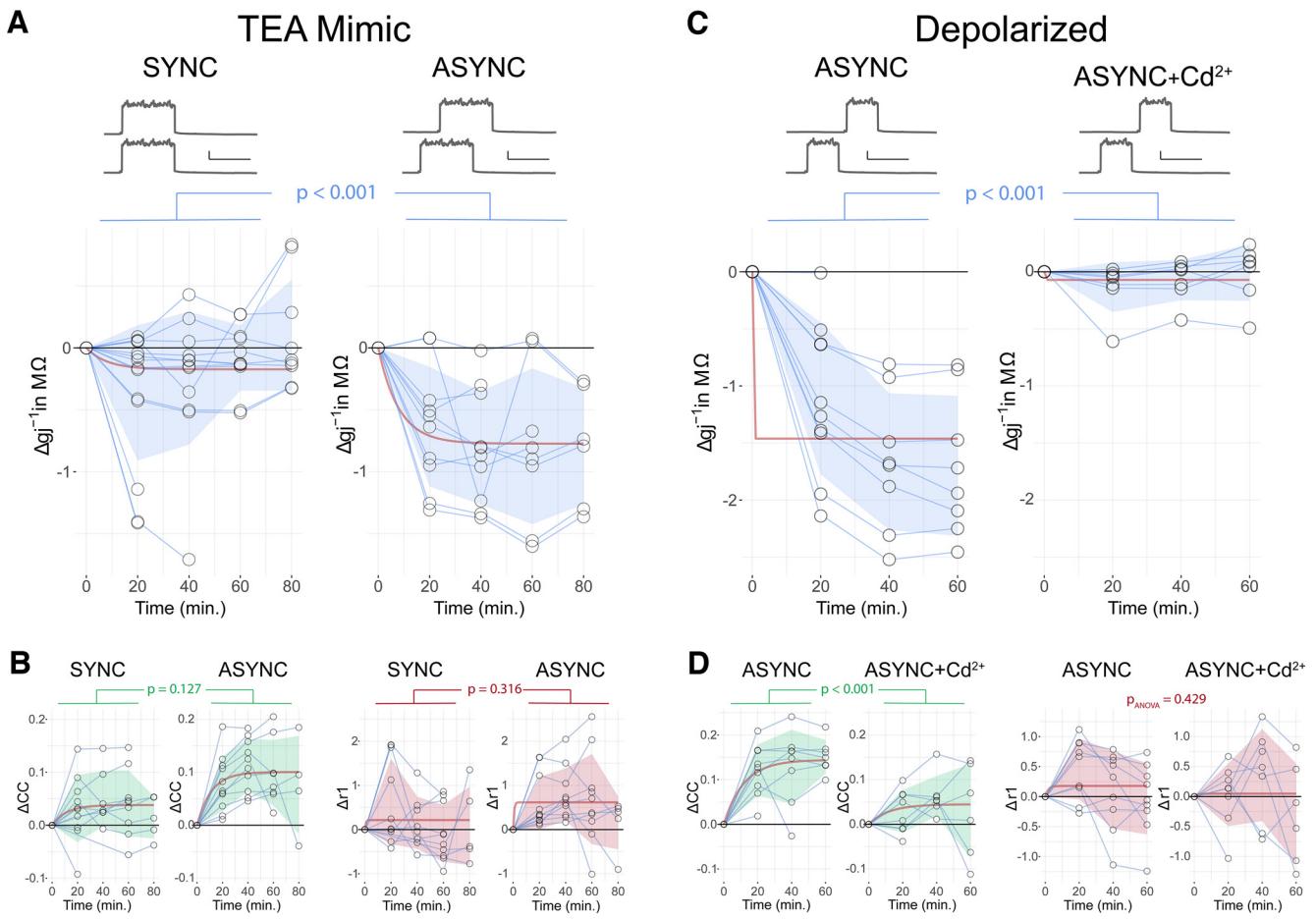

Figure 2. eLTP requires desynchronized activity and Ca^{2+}, not depolarization alone. Traces show the relative duration and overlap of applied stimuli (Fig. 1). ***A***, TEA Mimic stimuli (increased depolarization and duration) applied synchronously (SYNC) in coupled LCs result in little to no eLTP (i.e., a decrease in coupling resistance, expressed as Δg_j^{-1}). Asynchronous depolarization across gap junctions (ASYNC) results in a substantial eLTP that is significantly different from the synchronously applied stimulus ($p < 0.001$). Calibration: 10 mV and 1 s. ***B***, Although ANOVA revealed an overall effect (see below, Results), *post hoc* comparisons did not reach statistically significant values for coupling coefficient (ΔCC, $p = 0.127$) or membrane resistance (ΔR1, $p = 0.316$) between cells receiving the SYNC and ASYNC TEA Mimic stimuli. ***C***, Decreasing the duration of the depolarization relative to the TEA Mimic stimulus (Depolarized ASYNC) still results in a strong eLTP effect. However, potentiation does not occur with the same stimulus protocol in the presence of Cd^{2+} (Depolarized ASYNC+Cd^{2+}) resulting in a significant difference between this protocol with and without Cd^{2+}. These results indicate that calcium influx is required for this eLTP effect to occur. Calibration: 10 mV and 1 s. ***D***, The Depolarized ASYNC protocol also results in a significant increase in coupling coefficient (ΔCC, $p < 0.001$), which also is abolished by the presence of Cd^{2+}. There was no significant effect of the Depolarized protocols on membrane resistance (ΔR1, $p = 0.429$). For all plots, circles connected by lines show change of a given parameter from baseline for an individual cell over time. Shaded regions denote SD. Red lines show the asymptotic regression fit with a fixed time constant for paired experimental protocols; *p* values report results of *post hoc* pairwise comparisons after significant main effects via ANOVA for all comparisons (see below, Results) except for ΔR1 for the Depolarized protocols, which did not warrant *post hoc* testing. For this parameter we report the *p* value of the ANOVA directly.

controlled before modeling. Resistances were constrained to be nonzero and positive, coupling coefficient was constrained to be between 0 and 1, and each comparison point exceeding a threshold beyond the median was excluded. The threshold was set as the largest inner quartile range for all time by condition groups in the data under consideration.

Statistical modeling. To compare the differences in dependent variables at steady state, we used a robust asymptotic regression fit on the change from baseline. We are interested specifically in the difference between asymptotes between groups. We allowed asymptotes to vary between groups while not allowing time constants to vary between groups. As a result, this model allows for a comparison of the effect of a treatment at steady state without prior knowledge of when the system has reached steady state. These models are fit using the drc library (Ritz et al., 2015) in R software. Whether a main effect is present is determined through ANOVA between an asymptotic model lacking group-specific asymptotes and a model with group-specific asymptotes. If the simpler model was unable to converge, as was the case in fitting ΔCC for the naturalistic protocols, this step was skipped. If a main effect was found, we tested for a difference in the asymptotes with a pairwise parameter ratio *post hoc* test based on the *t* statistic. In comparisons with more than two groups we adjust *p* values with the Holm procedure and report these as p_{adj}. If contrasts between groups could not be calculated, as was the case for ΔR_1 for the naturalistic protocols, we used a regression model followed by Tukey's *post hoc* test instead.

Dynamic clamp data processing. Our goal with these dynamic clamp experiments was to measure the similarity of a burst in one cell to that of a coupled cell and to the cell's expected baseline activity. We extracted the relevant voltage traces using the readABF library (https://CRAN.R-project.org/package=readABF) and used custom R functions. To find all instances where both networks were active simultaneously, we used the following approach. First, all time points where the voltage of an extracellular recording exceeded three times the inner quartile range of the voltage above the mean were found. If two of these events occurred with a duration of 0.5 s, they were considered to be part of the same putative burst. Any putative burst with a duration of <0.1 s was discarded with the remainder being considered bursts. From this, overlapping bursts can be identified and Pearson's correlation coefficient can be calculated to measure waveform similarity. Additionally, the difference in start times, the delay in burst onset, can be measured allowing

for examination in how similarity is affected by not only artificial coupling strength but delay as well.

Measuring similarity relative to control activity is not as straightforward. Control cardiac ganglion waveforms are variable within and between animals, which prevents both aligning a burst to reference control and subtracting the two to arrive at a robust estimate of the similarity to control bursts as a whole. To overcome this, we aligned each overlapping burst to every control burst and calculated the Pearson's correlation coefficient for the voltage of these. We retain the median correlation from each set to serve as the deviation from control activity for a given event. As with the above we examine these with respect to delay (see Fig. 4).

Visualizations. We relied on a combination of R plotting libraries (https://CRAN.R-project.org/package=lemon; https://CRAN.R-project.org/package=patchwork; https://CRAN.R-project.org/package=cowplot; https://cran.r-project.org/web/packages/ggrepel/index.html) to visualize the data produced for these experiments. Minor aesthetic adjustments were made with Adobe Illustrator.

Data availability

Both the data and code associated with these analyses are available on request from the corresponding author.

Results

TEA Mimic protocol requires lack of synchrony and Ca^{2+} to increase coupling

TEA application is known to increase LC depolarization and decrease network synchrony (Lane et al., 2016) in cardiac ganglia. These findings became the foundation for our first set of experiments where we tested whether increased depolarization sufficed to change coupling, or whether desynchronization also was necessary. To do so, we developed a current injection protocol that mimicked the depolarization effects seen by Lane et al. (2016) and applied this either synchronously (Sync) or asynchronously (Async). The group exposed to the desynchronized TEA Mimic protocol exhibited a rapid decrease in coupling resistance relative to baseline (Δg_j^{-1}) that represents an increase in coupling strength (eLTP), whereas the synchronous group did not (Fig. 2*A*). We find a significant difference between the steady state of these groups for g_j^{-1} (Δg_j^{-1} TEA Mimic Sync versus TEA Mimic Async, df = 1, $F = 36.176$, $p < 0.0001$, ANOVA; TEA Mimic Sync vs TEA Mimic Async, df = 103, $t = -4.871$, $p < 0.0001$). There was significant main effect of the TEA Mimic protocol on coupling coefficient (ΔCC, df = 1, $F = 23.908$, $p < 0.0001$, ANOVA) and membrane resistance (ΔR_1 TEA Mimic Sync versus TEA Mimic Async, df = 1, $F = 6.480$, $p = 0.013$, ANOVA). However, *post hoc* comparisons (Fig. 2*B*) did not reach statistical significance between the synchronous and asynchronous groups (ΔCC, TEA Mimic Sync vs TEA Mimic Async, df = 87, $t = -1.540$, $p = 0.127$; ΔR_1, TEA Mimic Sync vs TEA Mimic Async, df = 92, $t = -1.001$, $p = 0.316$).

We generated a variant of this asynchronous protocol with a shortened depolarization relative to the TEA Mimic (matching the length of a control burst) but maintaining the high amplitude and asynchrony. This Depolarized (Depol) protocol (Fig. 1*C*) has no overlap between the activation of the cells protocol (Fig. 2*C*). We noted similar changes in coupling relative to the TEA Mimic despite halving the length of the depolarization (Fig. 2*C*). When we visually compared the asynchronous Depolarized and TEA Mimic protocols (Fig. 2*A*,*C*), both result in increased coupling. Furthermore, we find that the estimated asymptote for this treatment differs from zero (Δg_j^{-1} Asymptotic regression, df = 62, $t = -16.844$, $p < 0.0001$).

To determine whether the observed increase in coupling is dependent on calcium influx through voltage-dependent channels, we applied the depolarized asynchronous protocol in the presence of extracellular $CdCl_2$ (250 μM). Blockade of calcium influx during the stimulus protocol virtually eliminated the increase in coupling seen as a result of the asynchronous Depolarized protocol (Fig. 2*C*). These groups differ significantly in the change in coupling resistance (Fig. 2*C*) and coupling coefficient (Fig. 2*D*; Δg_j^{-1}, df = 1, $F = 133.484$, $p < 0.0001$, ANOVA; Δg_j^{-1} Depol Async vs Depol Async with Cd^{2+}, df = 62, $t = -28.058$, $p < 0.0001$; ΔCC, df = 1, $F = 33.133$, $p < 0.0001$, ANOVA; ΔCC Depol Async vs Depol Async with Cd^{2+}, df = 60, $t = -12.785$, $p < 0.0001$) but did not experience a change in membrane resistance (Fig. 2*D*; ΔR_1, df = 1, $F = 0.635$, $p = 0.429$, ANOVA).

A naturalistic waveform increases or decreases coupling based on the delay between cells

To test whether these findings hold with a more naturalistic stimulus, we used a protocol derived from a single control LC waveform applied at four phase angles of 0, 22.5, 45, and 90° (~0.00, 0.24, 0.49, 0.98 s representing an offset of 0, 1/16th, 1/8th, and 1/4th of the period; Fig. 1*C*,*D*). Below a threshold of 90°, we observed potentiation of the synapse as measured by an overall decrease in g_j^{-1} (Fig. 3*A*). We find a significant effect of phase on Δg_j^{-1} ($F = 38.665$, df = 3, $p < 0.0001$, ANOVA) and at 90° results in an increase in coupling resistance (eLTD) that differs significantly from all other groups (Δg_j^{-1} 0 vs 90°, df = 176, $t = -27.220$, $p < 0.0001$, $p_{adj} < 0.0001$, asymptotic regression), (Δg_j^{-1} 22.5 vs 90°, df = 176, $t = -10.789$, $p < 0.0001$, $p_{adj} < 0.0001$, asymptotic regression), (Δg_j^{-1} 45 vs 90°, df = 176, $t = -10.036$, $p < 0.0001$, $p_{adj} < 0.0001$, asymptotic regression).

We found no effect of the naturalistic stimuli on coupling coefficient (ΔCC, $F = 38.665$, df = 3, $p = 0.99$, ANOVA; Fig. 3*B*). We were unable to calculate contrasts in ΔR_1, possibly because of insufficient saturation, so we used a linear model with time by phase and an interaction effect instead. We make limited interpretation of these data, which suggest an effect (ΔR_1, df = 4, $F = 4.804$, $p = 0.001$, ANOVA) but suggest that 0° is distinguishable from 45°, but 22.5 and 90° are indistinct from these two (Fig. 3*C*).

Taking the above experiments together, the results are consistent with a lack of synchrony being responsible for altering coupling resistance (Figs. 2, 3). However, it appears that phase alone is insufficient to fully predict all cases where this will occur. as Depolarized Async and Naturalistic 90° possess similar delays and periods with depolarization differing between the two protocols. Despite having the same phase angle, at different levels of depolarizations the sign of gap junction regulation is flipped, resulting in eLTP in some circumstances and eLTD in others. This observation supports a role for another electrophysiological factor, such as depolarization amplitude or duration, to interact with synchrony in influencing coupling.

Dynamic clamp reveals a detrimental effect of coupling strength and delay on target output of cells

The goals of this experiment were twofold. First, to determine the effects of coupling strength on synchrony between two cells with a continuous range of delay times in their relative activities. This is accomplished by comparing the activity of two artificially coupled cells in two ganglia across a range of coupling conductances. The second was to investigate how coupling and delay interact to pull the cell out of its normal pattern of activity and to test for a delay-dependent cost to the cell that is minimized by

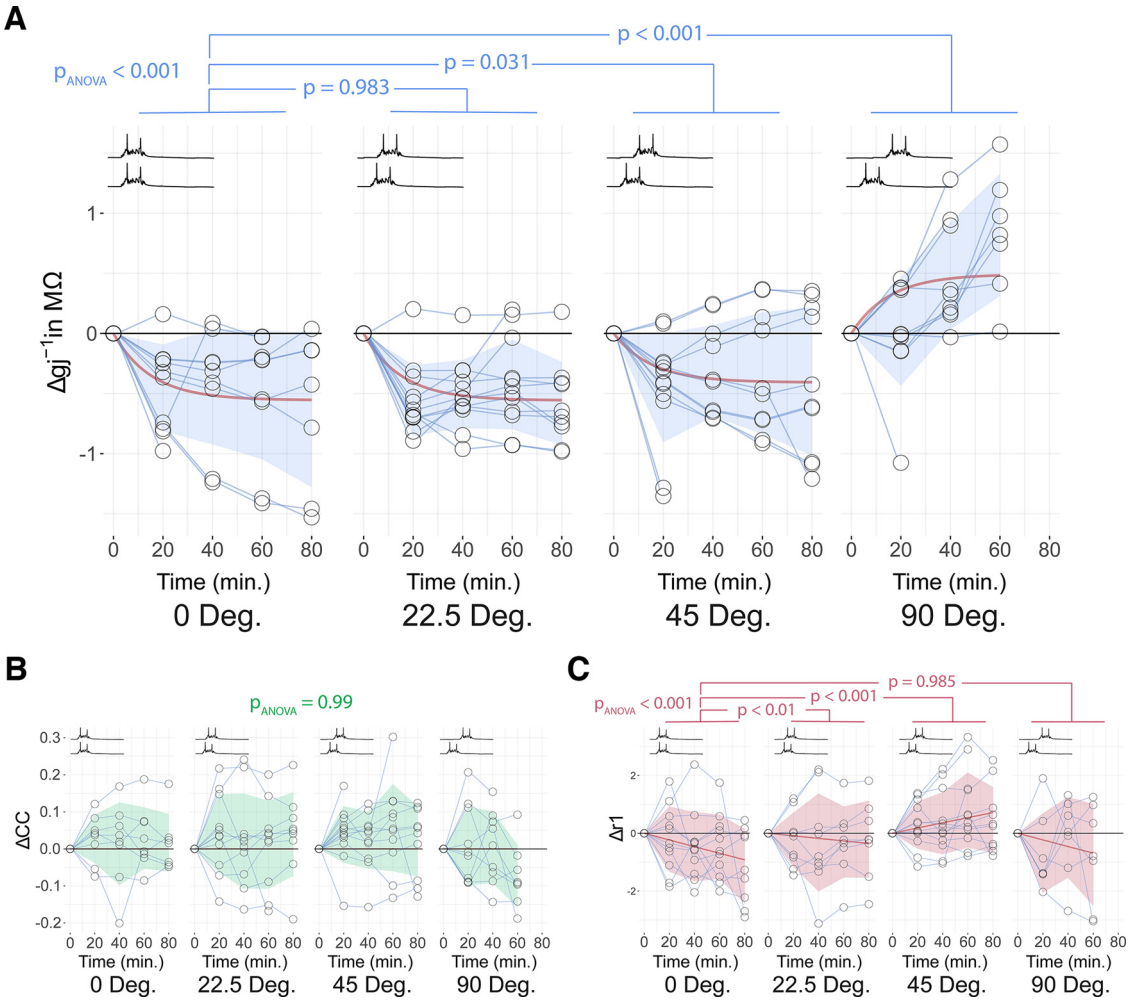

Figure 3. Desynchronization with a naturalistic stimulus at 90° phase shift depresses the LC 4/5 electrical synapse; shortened delays potentiate the synapse. We used the Naturalistic waveform to examine the effects of asynchronous stimulation at more normative voltages. ***A***, At these more normative voltages across a range from 0–90°, there is a significant main effect on Δg_j^{-1} ($p_{ANOVA} < 0.001$). The sign of change for Δg_j^{-1} (i.e., eLTP or eLTD) appears dependent on the magnitude of delay. A naturalistic waveform applied with a delay <90° (i.e., an offset of one-fourth the period between cells) results in eLTP, whereas a delay of 90° results in eLTD. There is also a seeming dose-dependent effect on this change as *post hoc* comparisons show no difference between 0° and 22.5°, whereas both 45° ($p < 0.05$) and 90° ($p < 0.001$) are significantly different from the synchronously applied stimulus (0°). ***B***, There was no significant main effect for changes in coupling coefficient with the naturalistic stimulus ($P_{ANOVA} = 0.99$). ***C***, However, a significant effect on membrane resistance was found ($p_{ANOVA} < 0.001$). For all plots, circles connected by lines show change of a given parameter from baseline for an individual cell over time. Shaded regions denote SD. Red lines show the results of asymptotic regression fit with a fixed time constant across all four groups; *p* values report results of *post hoc* pairwise comparisons between the control (0°) and each phase shift condition when a significant main effect was detected. Inset, Traces show the relative duration and overlap of applied stimuli (Fig. 1).

electrical synapse potentiation or depression. This cost is measured by comparing a the activity of a cell with varied coupling strength and delay with its own baseline activity (i.e., without artificial coupling), in effect quantifying deformation from the expected activity.

To use a truly naturalistic voltage stimulus, we used dynamic clamp to take advantage of endogenous cell activity in a manner that provides a near continuous range of delays and complete control over coupling properties. To do so, we introduced a simulated gap junction between two LCs in separate, active CGs (Fig. 4*A*) and recorded LC activity from both networks under six artificial synaptic strengths (0, 0.025, 0.05, 0.1, 0.15, and 0.2 µs). Using the extracellular activity of a network (Fig. 4*B.i*) bursts can be identified (Fig. 4*B.ii*). The delay is used as one independent variable (Fig. 4*B.iii*), with the period of a cell's activity being used to compare deformation from baseline (Fig. 4*C.i,ii*) and the overlap being used to compare the activity of the two networks (Fig. 4*D.i,ii*).

Recordings of each treatment were sufficiently long (115–300 s) to gain a roughly continuous sampling of delays between the preparations. To visualize the deviation from control activity, we plotted the median correlation coefficient, adapted from methods previously reported (Lane et al., 2016) between a burst (Fig. 4*C.i*, blue traces, A) and all control bursts (Fig. 4*C.i*, black traces, A, showing the first and last control burst, ellipsis representing all other control bursts), with respect to delay for a given coupling conductance (Fig. 4*C.ii*, translucent points are individual correlations, red point is the median). With these data we also examined how well artificially coupling two cells can promote more synchronous activity between cells across networks. Correlation between voltages of the overlapping time points (Fig. 4*B.ii,iii*) from network A and network B is calculated (Fig. 4*D.i*, A and B) and plotted as a function of delay for a given coupling conductance (Fig. 4*D.ii*).

We performed this experiment for one pair of CGs with naturally similar LC depolarization amplitudes (Fig. 5, Experimental Set 1) and one pair of networks consisting of LCs with naturally varying depolarization amplitudes (Fig. 5, Experimental Set 2). We assess the similarity in activity between the activities of the

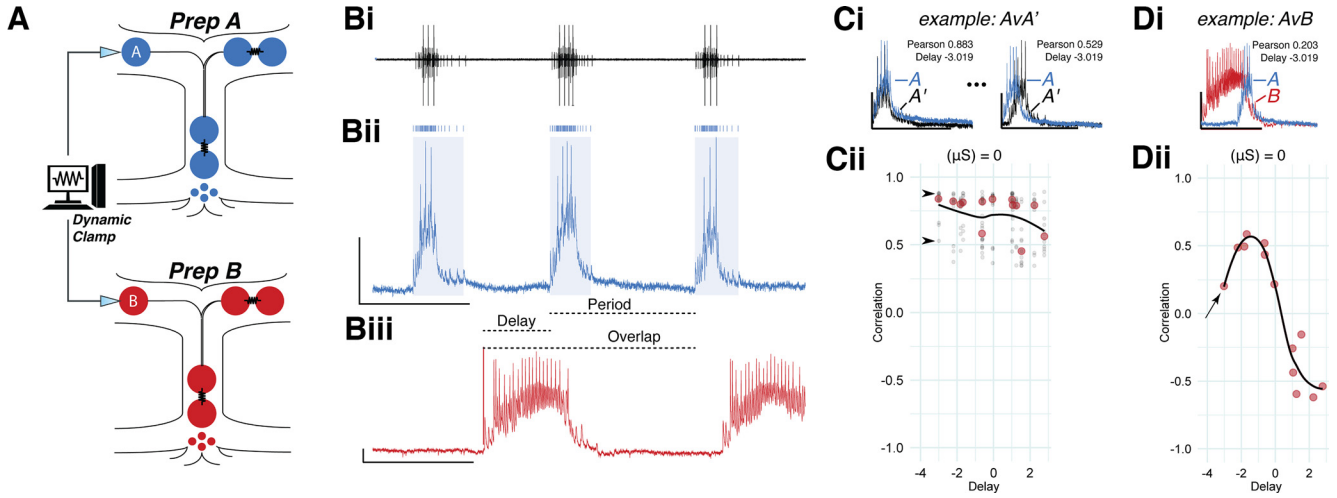

Figure 4. LC output is altered by phase delay in a coupling-conductance-dependent manner. ***A***, Using dynamic clamp, we artificially coupled two LC motor neurons from two different networks (i.e., animals) with their distinct ongoing rhythms intact. The simulated reciprocal synapse had a strength between 0 and 0.2 μS. ***B.i,ii***, Simultaneous extracellular (***B.i***) and LC intracellular (***B.ii***) recordings from a network (Prep A shown in blue) are used to define the depolarized phase of a LC (shaded in blue) based on the extracellular events (blue tick marks). ***B.iii***, We use the naturally occurring variation between preparations as an experimental tool. Preps A (in blue) and B (in red) exhibit endogenous activity with different cycle periods. Thus, over a sufficiently long time, the artificially coupled LCs experience activity with an approximately continuous range of positive and negative delays. Delay was calculated as the difference in the burst start times for two bursts across Prep A and Prep B relative to one another, with start times defined by Pacemaker (Small Cell) spikes (***B.i***, ***B.ii***, Fig. 1*B*, Trunk). Small Cell spikes were also used to calculate the period and duration of a given cycle. ***C.i,ii***, To measure similarity to the baseline activity of each cell while accounting for a variability of a cell at baseline, each burst is correlated with every burst of the control activity of its own network (i.e. with no coupling; ***C.i***) and a Pearson correlation coefficient determined. We refer to this comparison of a given burst (***A***, ***C.i***, blue trace) versus all bursts in the recorded baseline activity (A′, ***C.i***, black traces) in Prep A as AvA′ for the focal (A) and baseline (A′) traces, respectively. The two example baseline traces (A′) shown are those with the highest and lowest correlation in the set. As expected, when comparing bursts within a network with conductance set at 0 μS, this results in a fairly high correlation value (e.g., 0.883). The ellipses represent the complete set of A′ traces. ***C.ii***, This set of correlations is then plotted for a given delay between Prep A and B (Delay, ***B.iii***). Correlations from the example traces in ***C.i*** are shown with arrowheads. The median of a set of correlations (large red circle at a given value of delay) represents the similarity between bursts relative to the control activity of the network. When no artificial coupling is present (as in ***C***), this analysis results in a measure of how repeatable and consistent ongoing bursts are within a given network, where a score of 1.0 represents absolutely identical activity from burst to burst. Fitting these data allows us to see how correlation relates to delay across a population of bursts at a given level of conductance. ***D.i***, When instead the co-occurring bursts of two different networks are correlated (AvB), we can get a measure of the similarity of two LC waveforms across networks. These two cells have substantially different waveforms and thus a fairly low correlation value (0.203). ***D.ii***, Plotting and fitting a population of bursts across a range of delays demonstrates that cells in different preparations have a delay-dependent similarity (i.e., delay aligns or misaligns waveforms) and overall lower similarity than bursts within their respective networks. In this instance, these two preps have virtually no similarity in their waveforms (correlation = 0) at a delay of zero. The correlation value for the cells in ***D.i*** is indicated in the plot by the arrow and also demonstrates a delay at which there is little similarity or overlap in their waveforms. If changes in artificial coupling strength affect the similarity of bursts between Prep A and Prep B, the relationship between correlation and delay will be altered.

two networks with respect to delay and coupling conductance (Fig. 5, AvB). To aid in visualizing the trends with respect to conductance, the minimum, mean, and maximum correlations are shown for each conductance, without considering delay, in the far right graph. To assess the activity of each network to the control activity of the network, we visualize the median correlation of baseline activity (Fig. 4*C.ii*) with respect to delay and conductance for network A (Fig. 5, AvA') and network B (Fig. 5, BvB'). Descriptive statistics are plotted in the same format as for AvB.

We find that in both trials, the correlation coefficient between the networks (i.e., similarity to each other, not to a control output) was maximized by a high coupling conductance (Fig. 5, AvB). This was expected and serves to confirm that the system was operating correctly. We found in both trials that the self-similarity (i.e., correlation against the baseline activity of a cell) decreased with increased coupling conductance and that this effect appears more severe as the delay between networks increases (Fig. 5, AvA' and BvB'). In other words, the stronger the synapse between two cells and the longer the delay, the activity of a given cell will be less similar to its own baseline activity (measured as a correlation coefficient). Although output correlation was affected by coupling conductance in a somewhat linear manner (Fig. 5, descriptive statistics plots), delay affected correlation in a nonlinear manner (Fig. 5, AvA', BvB'). This relationship was inverted by switching the reference cell, thereby turning a negative delay positive (Fig. 5, compare delay that minimizes correlation between AvA' and BvB'). Finally, we observed that when cells were mismatched in excitability, there were pronounced differential sensitivities between cells (Fig. 5, Experimental Set 2, AvA' and BvB', compare shape of trends).

Discussion

The goals of this study were twofold. First, we set out to determine whether plasticity of electrical synapses can be induced solely by activity-dependent means (e.g., a transjunctional voltage) and second to shed light on the functional importance of coupling modulation in highly synchronous networks. This required a model system in which one can observe and maintain natural synchronous activity among constituent neurons and completely control neuron activity with voltage clamp. With the crustacean cardiac ganglion, we achieved the experimental control necessary to decouple activity from other network parameters to demonstrate a purely activity-dependent modulation of coupling that is directionally dependent on the degree of difference in activity between the coupled cells. We then performed artificial coupling experiments to explore how eLTP can help restore synchrony in a presumably compensatory fashion. However, we also show that after a point, increased coupling alone fails to prevent divergence from synchrony, at which we suggest it becomes advantageous for networks to cut off the aberrant cell through eLTD, salvaging the output of the remainder of the network.

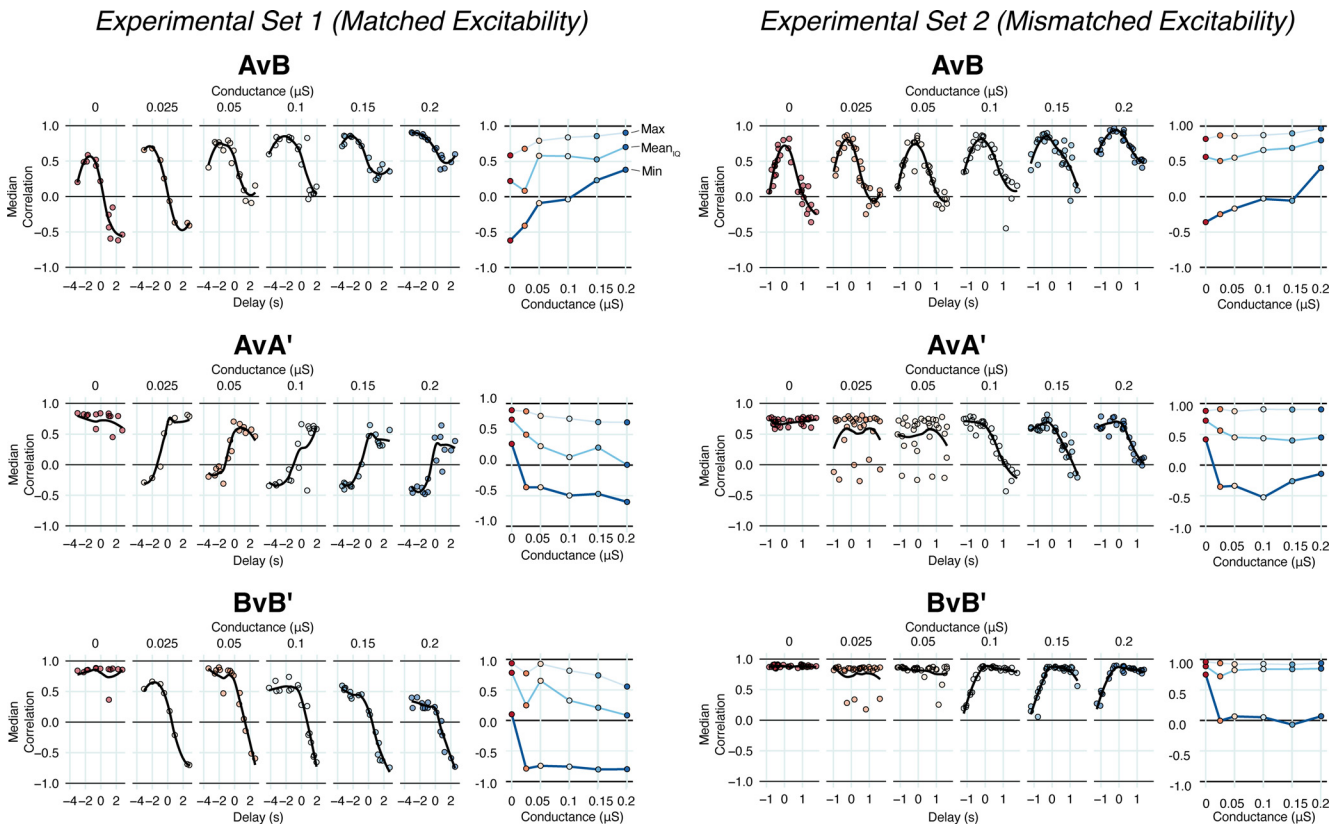

Figure 5. LC output is impaired by delay in a coupling conductance-dependent manner. We then tested two different Experimental Sets with hybrid networks of LCs artificially coupled across two preparations. One experiment featured cells across networks that had overall similar excitability (Experimental Set 1, Matched Excitability), and the other paired cells with overall dissimilar excitability (Experimental Set 2, Mismatched Excitability). Both hybrid networks display the same trend with different sensitivities to delay and coupling strength. In both cases, LC burst similarity between the artificially coupled preparations increases with increased coupling. Delay alters this relationship in a nonlinear fashion. AvB in both Experimental Sets represents the similarity between two artificially coupled cells between preparations (Prep A vs Prep B). These plots are the equivalent as those described in Figure 4*D*. These data show that both delay and coupling strength (G_{syn} from 0 to 0.2 µs, at top) alter burst similarity. The maxima and sensitivity to delay appears to differ across cell pairs. Right, To better visualize the effects of the artificial synaptic conductance strength, the maximum (Max), minimum (Min), and the Mean Interquartile ($Mean_{IQ}$) values for correlation (without accounting for delay) are tracked with varying dynamic clamp conductance. These data demonstrate that overall, increasing coupling conductance is able to increase waveform similarity between two cells, but the efficacy varies in a delay-dependent manner. AvA′ and BvB′ in both preparation sets represent the consistency of the artificially coupled cells activity relative to the ongoing activity in their own networks as a function of artificial coupling strength. These plots are the equivalent as those described in Figure 4*C* and represent the similarity scores of each cell (A or B) to its own baseline output (A′ or B′, respectively) as a function of G_{syn} and delay. Individual cells are differentially sensitive to the activity of their partner, and the hybrid network in Preparation Set 1 appears more sensitive than that of Preparation Set 2. When G_{syn} is 0 (no artificial synapse), waveform output for a given cell is consistent over time (i.e., across Delay). Delays closer to zero result in less loss of similarity to baseline activity. Right, To better visualize the effects of the artificial synaptic conductance strength, the Max, Min, and the Mean Interquartile ($Mean_{IQ}$) values for Correlation (without accounting for delay) are tracked with varying dynamic clamp conductance and demonstrate an overall decrease in similarity with increased coupling strength. In other words, as synapse strength is increased, each cell is more and more pulled out of its endogenous waveform as a function of both the delay between cells and the strength of the synapse. Each cell in a hybrid network shows the opposite pattern to its partner (e.g., decreasing at positive delays vs decreasing at negative delays; contrast AvA′ and BvB′) as a positive delay from the vantage point of one network will be a negative delay from the other and because bursts are not symmetrical.

Loss of synchrony, and not increased depolarization, induces eLTP in LCs

Previous work demonstrated eLTP in crustacean cardiac ganglia, resulting from exposure of LCs to TEA, which causes not only hyperexcitability and increased depolarization (Ransdell et al., 2012, 2013) but also loss of synchrony among LCs (Lane et al., 2016). These experiments did not determine whether the salient signal inducing eLTP was increased activity of the TEA-exposed LCs or the loss of coordinated activity (or both). In this study, we find increased depolarization alone is insufficient to alter coupling (Fig. 2). Instead, a delay between depolarizations is required. This is repeated in three different experiments (Figs. 2, 3) with protocols that vary in the level of depolarization, and the phase delay between cells. Phase delay can elicit coupling modulation and is abolished by calcium channel blockade (Fig. 2*B*), which agrees with previously reported activity-dependent gap junction plasticity (Welzel and Schuster, 2018; Fricker et al., 2020). These experiments are consistent with the hypothesis of a voltage-delay-induced, calcium-mediated mechanism of electrical synapse potentiation (Haas et al., 2016). However, we do not yet know whether a meaningful differential in calcium forms across the synapse in the CG as seen when one coupled cell is driven in the mouse thalamic reticular nucleus (Fricker et al., 2020), acting as the salient signal, or whether this effect is driven by a different signal.

The magnitude of phase difference may determine whether eLTP or eLTD is induced

Here, for the first time to our knowledge, we find the same depolarizing stimulus produces both eLTP and eLTD, dependent on the amount of delay between cells. This appears as a phase by time interaction effect in our model, seen clearly in Figure 3. We observed clear and widespread eLTD with the Naturalistic stimulus at a phase angle of 90°. It appears that the point at which the

system switches from eLTP to eLTD may be smaller than 90° as some individual preparations also displayed eLTD at 45°. Furthermore, we are not ruling out a potential interaction with depolarization. For example, the stimulus protocols seen in Depolarized Async (Fig. 2*C*) and Naturalistic 90° (Fig. 3) have similar timings, with virtually no overlap in the activation of the two cells but differ substantially in their depolarization amplitude and result in eLTP and eLTD, respectively. Indeed, in general our most robust eLTP effects were elicited by our protocols that depolarize more (Figs. 1*C*, traces, 2, effects, compared with Fig. 3). It seems likely based on our data that magnitude of membrane depolarization may play a meaningful role in influencing synaptic plasticity in this system. A study from Fricker et al. (2020) is consistent with this hypothesis. They report when stimulation of TRN neurons evokes spiking that eLTP is induced, whereas evoked bursting and subsequent higher intracellular calcium results in eLTD. Our work suggests regulation may involve the sustained existence of a calcium gradient, but additional studies will be necessary to indicate the precise intracellular triggers of eLTP and eLTD.

Coupling conductance increases sensitivity of cell output to phase delay

Excitatory neuromodulators (Cruz-Bermúdez and Marder, 2007; Lane et al., 2018) or ionic current blockers (Ransdell et al., 2013; Lane et al., 2016) suppress coordination between LC neurons. This loss of synchrony is attenuated (Lane et al., 2016) or prevented (Lane et al., 2018) with an associated increase in coupling. This does not explain the utility of a biphasic response where coupling resistance is decreased at small delays and increased at larger ones (Fig. 3). Using hybrid networks formed between LCs of two different ganglia with an artificial electrical synapse, we tested for changes in cell output as an effect of delay between neurons and coupling conductance (Fig. 5). The logic of the experiment is as follows. First by comparing the activity of two artificially coupled cells in two different ganglia across a range of coupling conductances, we can determine how well coupling is able to promote more synchronous activity between (naturally variable) cells. We predicted that with smaller delays between the onset of activity of these two cells, increased coupling would increase their synchrony. However, at larger delays, not only would strong coupling likely be ineffective at synchronizing cell activity but it may also produce aberrant cell activity (relative to the home networks of cells). This leads to the second aspect of the logic of this experiment. By comparing the effects of experimentally varied coupling and delay on a the activity of a cell relative to its own baseline activity (i.e., artificial coupling of 0 μs), we demonstrate how coupling and delay may interact to pull the cell out of its normal pattern of output. We predicted that at some level of delay, it would become advantageous to reduce coupling, minimizing disruption of the natural activity of each cell.

These inter-related predictions were supported by the data (Fig. 5). The waveforms of artificially coupled cells are most similar under conditions of high coupling conductance and low delay in activity between the cells. In other words, when the activity of two dissimilar cells are not too different from one another, increased coupling can help converge on a common output. Conversely, when we look at these data from the perspective of the native biological network of each cell, we indeed find that the output from an artificially coupled cell is substantially altered from its baseline in a coupling and a delay-dependent manner, where longer delays and strong coupling cause the largest deviation (Fig. 5). This occurs even at coupling levels typically found in populations of these networks. When coupling is reduced to lower than typical biological levels (i.e., mimicking eLTD), this exerts a protective effect whereby a cell is no longer pulled from its typical pattern of activity by an artificially coupled partner with a high amount of delay. In other words, when the activity of two cells is highly dissimilar to one another (and the goal is synchrony), it is advantageous to decouple from a synaptic partner to try to maintain a pattern of activity.

Together, these experiments support the idea of a nonlinear cost to the output of a network, whereby a cell with disrupted activity within a network may be pulled back in to normal synchrony through electrical synaptic potentiation, but a severely impaired cell can be cut off from the remaining healthy cells via synaptic depression if its activity onset differs too greatly. How this decision to rescue or abandon an improperly behaving cell is determined remains a compelling question for future experimentation, both computational and physiological.

Conclusion

Electrical synapse plasticity is present across taxa in both innexin- and connexin-based synaptic coupling (Haas et al., 2011; Lane et al., 2016; Welzel and Schuster, 2018). Despite the multiple means documented by which circuits can tune their electrical synapses, our data demonstrate that timing of voltage activity between two coupled cells can dynamically modulate electrical synapses. Further, with our study there is now combined evidence that this too is a calcium-mediated (Sevetson, 2017) and likely depolarization-dependent mechanism (Fricker et al., 2020), which is conserved across invertebrates and vertebrates. We suspect that the features that tune these properties will underlie the dynamics of long-term electrical synapse plasticity akin to what has been proposed for membrane excitability and demonstrated *in silico* (O'Leary et al., 2014). These mechanisms undoubtedly work in conjunction with other regulatory mechanisms of cellular and synaptic properties to provide robust constraints on network output.

References

Alcamí P, Pereda AE (2019) Beyond plasticity: the dynamic impact of electrical synapses on neural circuits. Nat Rev Neurosci 20:253–271.

Allen MJ, Godenschwege TA, Tanouye MA, Phelan P (2006) Making an escape: development and function of the *Drosophila* giant fibre system. Semin Cell Dev Biol 17:31–41.

Bennett MVL (1966) Physiology of electronic junctions. Ann NY Acad Sci 137:509–539.

Cooke IM (2002) Reliable, responsive pacemaking and pattern generation with minimal cell numbers: the crustacean cardiac ganglion. Biol Bull 202:108–136.

Cruz-Bermúdez ND, Marder E (2007) Multiple modulators act on the cardiac ganglion of the crab, *Cancer borealis*. J Exp Biol 210:2873–2884.

Fricker BA, Heckman EL, Cunningham PC, Wang H, Haas JS (2020) Activity-dependent long-term potentiation of electrical synapses in the mammalian thalamus. J Neurophysiol 125:476–488.

Haas JS, Landisman CE (2012) Bursts modify electrical synaptic strength. Brain Res 1487:140–149.

Haas JS, Zavala B, Landisman CE (2011) Activity-dependent long-term depression of electrical synapses. Science 334:389–393.

Haas JS, Greenwald CM, Pereda AE (2016) Activity-dependent plasticity of electrical synapses: increasing evidence for its presence and functional roles in the mammalian brain. BMC Cell Biol 17(Suppl 1):14.

Kothmann WW, Trexler EB, Whitaker CM, Li W, Massey SC, O'Brien J (2012) Nonsynaptic NMDA receptors mediate activity-dependent plasticity of gap junctional coupling in the AII amacrine cell network. J Neurosci 32:6747–6759.

Lane BJ, Samarth P, Ransdell JL, Nair SS, Schulz DJ (2016) Synergistic plasticity of intrinsic conductance and electrical coupling restores synchrony in an intact motor network. Elife 5:e16879.

Lane BJ, Kick DR, Wilson DK, Nair SS, Schulz DJ (2018) Dopamine maintains network synchrony via direct modulation of gap junctions in the crustacean cardiac ganglion. Elife 7:e39368.

Marder E, Gutierrez GJ, Nusbaum MP (2017) Complicating connectomes: electrical coupling creates parallel pathways and degenerate circuit mechanisms: electrical coupling creates parallel pathways and degenerate circuit mechanisms. Dev Neurobiol 77:597–609.

O'Leary T, Williams AH, Franci A, Marder E (2014) Cell types, network homeostasis, and pathological compensation from a biologically plausible ion channel expression model. Neuron 82:809–821.

Ransdell JL, Nair SS, Schulz DJ (2012) Rapid homeostatic plasticity of intrinsic excitability in a central pattern generator network stabilizes functional neural network output. J Neurosci 32:9649–9658.

Ransdell JL, Nair SS, Schulz DJ (2013) Neurons within the same network independently achieve conserved output by differentially balancing variable conductance magnitudes. J Neurosci 33:9950–9956.

Ritz C, Baty F, Streibig JC, Gerhard D (2015) Dose-response analysis using R. PLoS One 10:e0146021.

Sevetson J, Fittro S, Heckman E, Haas JS (2017) A calcium-dependent pathway underlies activity-dependent plasticity of electrical synapses in the thalamic reticular nucleus: calcium and plasticity of electrical synapses. J Physiol 595:4417–4430.

Spray DC, Harris AL, Bennett MVL (1979) Voltage dependence of junctional conductance in early amphibian embryos. Science 204:432–434.

Wang S, Borst A, Zaslavsky N, Tishby N, Segev I (2017) Efficient encoding of motion is mediated by gap junctions in the fly visual system PLOS Comput Biol 13:e1005846.

Wang Z, Neely R, Landisman CE (2015) Activation of Group I and Group II metabotropic glutamate receptors causes LTD and LTP of electrical synapses in the rat thalamic reticular nucleus. J Neurosci 35:7616–7625.

Watanabe A (1958) The interaction of electrical activity among neurons of lobster cardiac ganglion. Jpn J Physiol 8:305–318.

Welzel G, Schuster S (2018) Long-term potentiation in an innexin-based electrical synapse. Sci Rep 8:12579.